EAC of Non-Sensitized Stainless Steel and of Alloy 600 Across a Range of LiOH vs KOH Estimated Crevice Chemistries

Peter Chou
Electric Power Research Institute
Palo Alto, CA 94304
USA

Peter Andresen
JLN Consulting
12204 Wildwood Park Place
Bakersfield, CA 93311
USA

Stuart Medway
Amentum UK
Walton House Laboratory
Birchwood Park, Warrington
United Kingdom

Frank Gift
Electric Power Research Institute
Palo Alto, CA 94304
USA

Keith Fruzzetti
Electric Power Research Institute
Palo Alto, CA 94304
USA

ABSTRACT

To address the significant vulnerability to a shortage of enriched Lithium-7 hydroxide (^{7}LiOH), EPRI has an on-going, multifaceted program in place to evaluate the addition of potassium hydroxide (KOH) instead of ^{7}LiOH for pressurized water reactor (PWR) primary pH control. The specific objective of this study is to assess whether the use of KOH significantly elevates the risk of environmentally assisted cracking of pressurizer heaters, across a range of estimated crevice chemistries; the specific materials of concern are Alloy 600 (representing Ni-base alloys) and Type 304/304L stainless steel (representing stainless steels). For Alloy 600, even at a concentration factor of 316, it is not possible to say on the basis of crack initiation time, determined by direct current potential drop (DCPD), that there is an appreciable difference in EAC susceptibility between the equimolar pair of LiOH and KOH crevice chemistries. For the stainless steel, comparing equimolar water chemistries at concentration factors of ~100 and above, higher crack growth rates are observed in the KOH-based water chemistry of an equimolar pair, correlating with faster crack initiation that occurs in the KOH-based water chemistry of an equimolar pair. At concentration factors of ~30 or lower, LiOH vs. KOH does not impact crack growth rates. Crack initiation tests in an equimolar pair of water chemistries at a concentration factor of 20 did not produce any initiations within the test duration. The combination of crack growth and crack initiation data, given the correlation between them, represents a compelling argument that no LiOH vs. KOH difference in crack initiation behavior should be expected at a concentration factor of 20, although direct comparison of initiation times is not possible.

Key words: Potassium Hydroxide (KOH), Lithium Hydroxide (LiOH), EAC (environmentally assisted cracking), crevice chemistry, crack growth, crack initiation

INTRODUCTION

To address the significant vulnerability to a shortage of enriched Li-7 hydroxide (^{7}LiOH), EPRI has conducted a multidisciplinary evaluation of the addition of KOH instead of ^{7}LiOH for PWR primary pH control including materials compatibility. The choice of KOH is guided by its use in Russian-designed VVER reactors. Adoption of KOH will release the plants from competition with other industries for ^{7}Li; KOH's stable supply removes an uncertainty that may negatively impact advanced planning of plant operations.

As early as 1999, EPRI Report TE-114158 [1] indicated: *"Sufficient data exists to indicate good compatibility between the Zr-based alloy fuel cladding and components and the KOH/H_3BO_3 coolant chemistry. VVER experience also indicates good compatibility with the KOH coolant and stainless steel (SS) components. However, the Ni-based alloys used in steam generators have not been extensively tested in KOH solutions, and evaluation of Stress Corrosion Cracking (SCC) concerns with these materials may be necessary prior to full plant implementation. This evaluation should include the assessment of crevice areas to assure avoidance of conditions where KOH may concentrate to levels deleterious to SCC performance."*

More recently, EPRI 3002005408 [2] conducted a review of the open literature and concluded, based on general data of KOH vs. LiOH and on the VVER experience, that the use of KOH is not expected to have significant effects on the structural materials of the reactor vessel internals, pressure boundary, and steam generators. However, it also notes that there is a lack of specific data, particularly with respect to Ni-base alloys (which are not used extensively in VVERs), to the local chemistry that may develop in crevices subject to a heat flux, and to occluded oxygenated environments.

The scope of EPRI's Materials Testing program, of which this investigation is a part, conducted due-diligence testing that directly ascertains KOH-based PWR water chemistry effects on SCC susceptibility relative to the conventional LiOH-based PWR water chemistry. Its scope was determined in discussion with EPRI's KOH Advisory Committee, comprised of industry experts from several different utilities (both PWRs and VVERs), as well as NSSS and fuel vendors. [3, 4]

This investigation is motivated by concern about the heated geometric crevice between pressurizer heater (sheaths) and their support plates, as it was considered by EPRI's KOH Advisory Committee as the most limiting PWR crevice location within which concentrated local chemistry may develop, driven by a temperature gradient and superheat.[1] Calculations indicate that the hydrogenated concentrated crevice chemistries have elevated pH, which increases susceptibility to environmentally assisted cracking ("caustic cracking"). EPRI's assessment of the operating experience of VVER and PWR pressurizer heaters, however, indicates performance has generally been good in properly manufactured heaters (acceptable levels of cold work and residual stress) with respect to environmentally assisted cracking, particularly for the VVER fleet [5]. Neither the VVER Materials Degradation Matrix nor the VVER Issue Management Tables identify caustic cracking of VVER pressurizer heater sheaths as a generic problem [6], [7]. The good overall operating experience of PWR pressurizer heaters may be most clearly illustrated by EDF's experience [8]. EDF conducted extensive evaluations of pressurizer heater failures to address cracking incidences that culminated in 22 heater sheath breaches by the year 2011 (compared with approximately 1200 electrical failures of heaters through the same operating period); 12 of the 22

[1] Electrochemically driven concentrated crevice chemistry does not occur because the electrochemical corrosion potential is low everywhere within the hydrogenated primary circuit of PWRs.

breached heaters were removed and evaluated in a laboratory setting, and IGSCC was confirmed as the degradation mechanism on 9 of these Type 316L stainless steel sheaths. The primary causal factor for the IGSCC was identified as high levels of cold work and residual stress in the heater sheath (although EDF included the possibility of elevated pH in its assessment). Fabrication practices of the replacement heaters were modified to incorporate induction annealing to reduce the cold work and residual stress; there have been no reported incidents of SCC degradation with these replacement heaters.

The specific objective of this study is to resolve uncertainty about whether the use of KOH significantly elevates the risk of environmentally assisted cracking of the pressurizer heaters, by conducting tests across a range of estimated (hydrogenated) crevice chemistries on Alloy 600 and 304/304L stainless steel, with limited testing of Type 321 stainless steel.

EXPERIMENTAL PROCEDURE

Water Chemistries

Table 1 provides the LiOH-based and KOH-based water chemistries used in this investigation. Subsequent discussion will often refer to a particular water chemistry by its "letter" in this table. The water chemistries are designed to be equimolar pairs with respect to Li [added as LiOH], K [added as KOH] and B [added as H_3BO_3]. The equimolar pairs are: (A, G), (B, H), (C, I), (D, J), (E, K), and (M, N). Crack initiation and crack growth of specimens of the same material (and heat) and cold work level were tested in selected pairs to compare their behavior.

A concentration factor (CF) of 254 was initially calculated for the solution inside the crevice vs. the bulk coolant by equating the mass of new potassium that enters the crevice and the amount of potassium that diffuses out [9]. The assumptions supporting the initial CF calculation included the following:

- Generic geometric and heat flux conditions representative of a variety of potential pressurizer configurations (for mass-flow calculations).
- The mass of new potassium entering the crevice is based on an end-of-cycle RCS water chemistry (see next paragraph), which replenishes the water leaving the crevice by boiling.
- Crevice boiling was assumed to not induce convection.
- Potassium was assumed to leave the crevice by back-diffusion only, following its build-up within the crevice.

The solution compositions of the water chemistry pair (E, K) in Table 1 were then calculated by applying a CF of 316 in the MULTEQ software with the "static" (vs. "flowing") and "steam retained" (vs. "steam removed") options,[2, 3] starting with representative end-of-cycle (EOC) water chemistries of [5 ppm B, 0.75 ppm Li] or [5 ppm B, 4.22 K], which are equimolar, as the atomic weight of K is 5.63X that of Li. A CF of 316, instead of 254, was used to accommodate step size constraints within the MULTEQ calculations.

- This CF of 316, which is the upper end of the range in Table 1, was selected to be extremely conservative (aggressive) for comparative crack initiation testing. It will be shown later that this choice was overly conservative and led to results that are incongruent with operating experience.

The solution compositions of the water chemistry pair (M, N) in Table 1 were similarly calculated by applying a CF of 20 in the MULTEQ software with the same "static" and "steam retained" options, starting with the same representative end-of-cycle (EOC) water chemistries.

---

[2] The static option is considered to be more representative of crevice concentration processes than the flowing model. The use of the steam retained option provided more stable results in the calculation.

[3] Sensitivity calculations showed that the effect of iron is limited. Iron and other transition metal corrosion products would be expected to be present in any high-temperature testing system. Therefore, from a practical perspective, no extraordinary measures to remove or exclude these species from the test solution should be necessary.

All of the other water chemistry pairs in Table 1 were derived from (E, K); while keeping the boron concentration the same, the pairs (D, J), (C, I), and (B, H) were made successively more dilute by a factor of ~3.2 in molar alkali concentrations; the dilution step from (B, H) to (A, G) was a larger factor of ~5.5, but the behavior in (A, G), the least concentrated pair, was not evaluated, based on results obtained from the other pairs. The CFs reported for these pairs were approximated by multiplying [the molar ratio of their alkali concentration to that of (E, K)] with [(E, K)'s concentration factor of 316]. As will be discussed later, crack growth rate testing used these water chemistry pairs to efficiently assess relative susceptibilities of stainless steels as a function of concentration factors.

For comparison, once convection associated with thermal differences and the flow of steam out of the crevice is included, the CF is calculated to be approximately 2. [10]

Table 1. LiOH-based and KOH-based Water Chemistries used in this investigation, designed to be equimolar pairs: (A, G), (B, H), (C, I), (D, J), (E, K), and (M, N). The behavior in (A, G), the least concentrated pair, was not evaluated, based on results obtained from the other pairs.

Chemistry		B (mmol)	Alkali (mmol)	B (ppm)	Li (ppm)	K (ppm)	Conc. Factor	(B/Alkali) [molar ratio]	(B/Alkali) [ppm ratio]	pH(T) 350°C
LiOH	A	13.25	0.1920	143.1	1.32	0	~1.75(3)	69.01	108	8.28
	B	13.25	1.05	143.1	7.26	0	~10(3)	12.62	19.7	8.88
	C	13.25	3.37	143.1	23.3	0	~30(3)	3.932	6.14	9.26
	D	13.25	10.78	143.1	74.4	0	~100(3)	1.229	1.92	9.68
	E	13.25	34.49	143.1	238	0	316(2)	0.3842	0.601	10.20
KOH	G	13.25	0.1920	143.1	0	7.51	~1.75(3)	69.01	19.1	8.30
	H	13.25	1.05	143.1	0	41.2	~10(3)	12.62	3.47	8.94
	I	13.25	3.37	143.1	0	131.7	~30(3)	3.932	1.087	9.34
	J	13.25	10.78	143.1	0	421	~100(3)	1.229	0.340	9.78
	K	13.25	34.49	143.1	0	1349(1)	316(2)	0.3842	0.1061	10.33
LiOH	M	2.16	2.05	23.4	14.2	0	20(2)	~1.06	1.65	9.32
KOH	N	2.15	2.09	23.2(1)	0	81.7	20(2)	~1.03	0.28	9.37

1. These values may differ by ~1% among (and within) this report and other references and are considered insignificant from calculation and testing perspectives.
2. Solution compositions were determined by implementing the CF within MULTEQ.
3. CF's were approximated by multiplying [the molar ratio of the alkali concentration to that of (E, K)] with (E, K)'s concentration factor of 316.

Crack Growth Rate Testing of Stainless Steel across a Range of Concentration Factors [Lucideon M+P Lab, USA]

Type 304 (heat AJ9139) and Type 321 (heat E6376) stainless steel pieces were forged to reduce the length by 20% ± 1% (in the rolling direction L of the original bar/piece), using a single press at 240°C to minimize deformation induced martensite; their compositions are provided in Table 2. The orientation of the two 1T CT (compact tension) specimens (one each of ~20% cold worked 304SS and ~20% cold worked 321SS) was S-L *vs. the forging direction*; i.e., the crack plane normal vector is parallel to the forging direction.

Table 2. Composition of the Type 304 and Type 321 stainless steels (wt%) used for crack growth rate testing. The same 304SS was used for crack initiation testing.

Alloy	Heat	Fe	C	N	P	S	Cr	Ni	Mo	Mn	Si	Ti
304	AJ9139	bal.	0.066	0.048	0.026	0.028	18.37	8.13	0.25	0.93	0.47	--
321	E6376	bal.	0.07	0.010	0.015	0.008	17.52	9.97	0.03	1.52	0.50	0.59

Water from a master supply preconditioned by ultrapure mixed bed demineralizers were used in all SCC systems. For the concentrated simulated crevice chemistries evaluated, no demineralizers were used in the water loops of the individual autoclave systems, because it would be difficult to equilibrate demineralizers, and they become inefficient in removing impurities. Without a demineralizer, the primary impurity in hydrogenated water is Fe^{2+}, which could be close to saturation in a real crevice; therefore, somewhat elevated levels of Fe^{2+} is not problematic in simulated crevice chemistries. At a sufficiently high pH in the crevice, Ni and Cr ions would also be present.

The SCC growth rate response was evaluated in a 4 L Hastelloy C-276 autoclave [because of the elevated pH of the water chemistries (Table 1)], at a flow rate of ~100 cc/min, 350°C, with on-the-fly changes in hydrogenated water chemistry in which nothing changed but the B/Li vs. B/K chemistry as the crack advanced. An aerated condition (2 ppm O_2) was used initially to promote SCC transitioning from the transgranular fatigue precrack to intergranular constant K, which was followed by a change to 19 cc/kg H_2 (1.7 ppm)[4] and the subsequent on-the-fly changes in water chemistry. The transitions in water chemistry were accomplished by mixing ~32 liters of the new solution in a separate, closed container, deaerating the solution with 100% hydrogen at atmospheric pressure (so during the chemistry transition the dissolved hydrogen was 17.7 cc/kg), then switching the inlet to the high-pressure pump to draw from the container. The dissolved hydrogen level was returned to 19 cc/kg after the ~32 L of solution was flushed through the system, and normal operation was continued. With ~3.6 L of solution in the autoclave, flowing 32 L of the new chemistry provide 15 autoclave volume exchanges at 350°C, which displace ~99.99997% of the prior chemistry from the autoclave and water board. The B and Li (or K) levels were continuously monitored by inlet and outlet conductivity, and by grab sample analysis for room temperature pH and residual impurities.

Crack length was monitored by DCPD in which current flow through the samples is reversed about twice per second, primarily to reduce measurement errors associated with thermocouple effects at all metal junctions and connections. An integrating nanovoltmeter (Agilent 34420A) was used to measure the ~100-200 μV DCPD potentials on the specimens with a typical resolution of <10 nV with averaging. In these studies on stainless steel, no resistivity compensation was used because very little resistivity shift occurs in stainless or carbon steels, or in high purity nickel alloys, versus some nickel alloys (e.g. Alloy 600), and does not bias the results significantly. [11] Zirconia sleeves in the CT specimen pin holes were used for insulation from the pins, clevises, and pull rods (which were machined from XM-19 stainless steel, UNS S20910). Additionally, within the autoclave, a zirconia washer insulated the upper pull rod from the internal load frame. The lower pull rod was electrically isolated from the autoclave using a Teflon lip seal and from the loading actuator using an insulating washer. Ground isolated instrumentation was used for the current supply and potential probe measurements.

SCC growth rate testing was performed using two 1T CT specimens in tandem (i.e., sharing the same loading string; Figure 1a): one ~20% CW 304SS and one ~20% CW 321SS. In the tandem arrangement, if crack growth rate responses of the two specimens with respect to stress intensity are comparable, then

[4] This is essentially the hydrogen concentration associated with the Ni/NiO equilibrium at 350°C, which is used for both Alloy 600 and stainless steels in this investigation, although for stainless steels, there is no change in SCC susceptibility in the vicinity of Ni/NiO.

the response of the two specimens will remain comparable throughout the test, thus providing two "duplicate" datasets in parallel. Unfortunately, the crack growth rate of these two specimens were significantly different, which led to the sequential collection of data; first by controlling the stress intensity factor of the Type 321 SS specimen, which had the faster crack growth rate, until its available ligament had been consumed, and it was removed from the autoclave; and then by controlling the stress intensity factor of the Type 304 SS specimen. Because the Type 304 SS had the lower crack growth rate, traversing its available ligament took a longer time, which offered more opportunities for on-the-fly water chemistry changes; therefore, there are more datapoints associated with the 304SS specimen than the 321SS specimen).

The electrochemical corrosion potentials (ECPs) of the specimens were monitored by a ZrO_2 membrane electrode (which depends on pH_T) and a Pt electrode (which depends on pH_T and H_2).

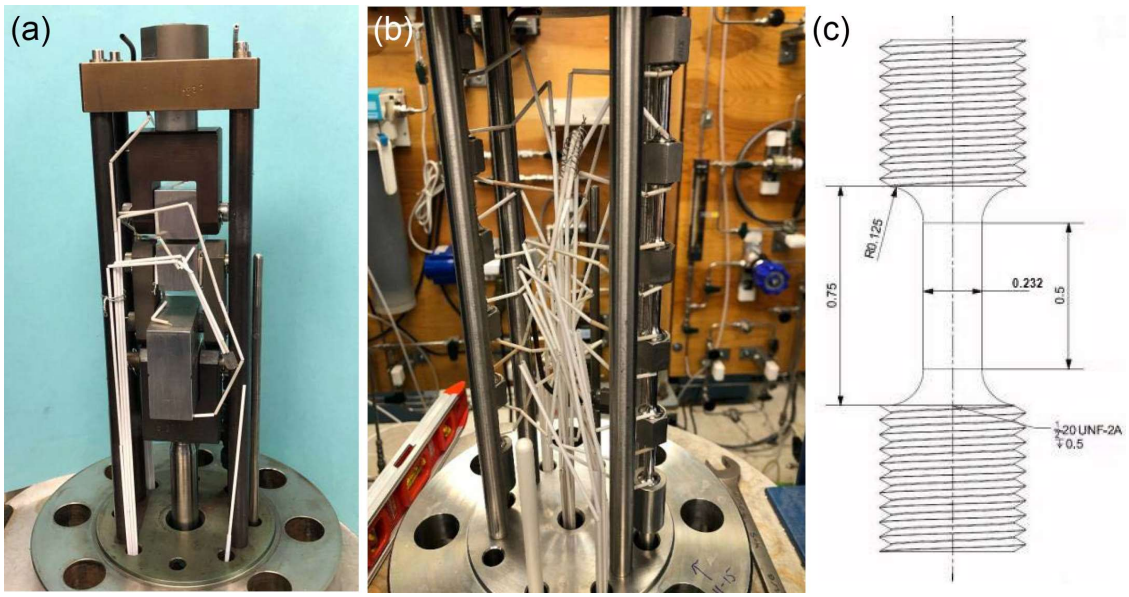

Figure 1. (a) 1TCT specimens assembled in the autoclave after air fatigue precracking. (b) Assembled crack initiation system. (c) Crack initiation specimen design (dimensions in inches); the total length of the specimen is 1.75 inches.

Crack Initiation Testing of Alloy 600 and Stainless Steel in Water Chemistry Pair (E, K; CF=316) [Amentum, UK]

The Alloy 600 material (heat #11415) was solution annealed then cold-forged to 15% thickness reduction in the longitudinal direction of the original product form (a ring forging); Table 3 and Table 4 provide the composition and the mechanical properties, respectively. It had been previously tested in a nominal PWR (LiOH-based) water chemistry as part of an international round robin [21]. The Type 304L material came from a hot-rolled plate (heat #71671) that was cold-forged to 15% thickness reduction in the S-direction of the plate; Table 5 and Table 6 provide the composition and the mechanical properties, respectively. The mechanical properties were used to determine the loads (consistent with specimen cross-sectional area) to deliver the target applied stresses in the crack initiation tests, which were referenced to the yield stress.

Table 3. Composition (wt%) of the Alloy 600 (heat 11415) used for crack initiation testing.

C	Si	Mn	Cr	Ni	S	P	Fe	Co	B	Cu	Al
0.036	0.20	0.20	15.53	74.6	0.001	0.005	8.87	0.03	0.002	0.03	0.27

Table 4. Tensile data in air at 340°C of the solution annealed and then cold forged Alloy 600 (heat 11415). "*" indicates the stress required to achieve the designated plastic strains. YS represents the yield stress and UTS the ultimate tensile strength.

Block N°	Specimen	Temperature (°C)	Young's Modulus (GPa)	0.2% YS (MPa)	*0.5% (MPa)	*1% (MPa)	UTS (MPa)
MT1249/22	APU07	340	190	410	455	495	630
MT1249/23	APU15	340	190	415	460	490	630

Table 5. Composition (wt%) of Type 304L stainless steel (heat 71671) used for crack initiation testing.

Fe	Cr	Ni	Mn	N	C	P	Si	S
bal.	18.400	8.108	1.899	0.0764	0.029	0.028	0.369	0.0005

Table 6. Tensile data in air at 340°C of the cold forged 304L stainless steel (heat 71671). "*" indicates the stress required to achieve the designated plastic strains. YS represents the yield stress and UTS the ultimate tensile strength.

Block No	Specimen	Temperature (°C)	Young's Modulus (GPa)	0.2% YS (MPa)	*0.5% (MPa)	*1% (MPa)	UTS (MPa)
MT643/70	APQ28	340	170	309	395	457	533
MT643/71	APQ36	340	160	307	390	454	533

The specimens used were a button head tensile specimen design shown in Figure 2a (40 mm long, 5 mm gauge diameter, and 18 mm gauge length); the gauge diameter is perpendicular to the direction of the 15% thickness reduction. The gauge section was polished progressively from 800 grit ISO paper, 6 µm diamond paste, to 1 µm diamond paste.

Identical tests were conducted in two nearly identical autoclaves systems, one for the LiOH-based water chemistry and one for the KOH-based water chemistry, each containing ten specimens. This enabled the tests to be run in parallel, and any alteration made to one test could also be made at the same time to its pair in the other chemistry. Corrosion resistant Hastelloy autoclave systems were used; the hot regions are fabricated from Hastelloy, while the cold regions are fabricated from Alloy 600.

For Alloy 600, in standard PWR primary water conditions, the SCC initiation susceptibility plateaus above the Ni/NiO transition [12] and the crack growth rate peaks around the Ni/NiO transition [13]. Therefore, in the crevice chemistry conditions, the hydrogen concentration [19.5 cc/kg H_2 (1.74 ppm)] was selected to be just into the Ni stable region in relation to the Ni/NiO transition to maximize susceptibility.[5] Although

[5] The Ni/NiO transition at 340°C is 15.3 cc/kg H_2 and at 350°C is 19.7 cc/kg, according to Eq. 2-2 in [14].

the Ni/NiO transition is not linked to the stress corrosion cracking behavior of stainless steel, the same hydrogen concentration was used.

The loading arrangement used for these tests is shown in Figure 2b. It is comprised of two chains of five specimens (10 specimens total) and a balance beam arrangement to connect the two chains to a single pull rod, which exits the autoclave through chevron seals and is connected to an Instron servo-electric testing machine. A catch system was used that can take up the load should a specimen fail. The specimens were electrically insulated from the grips by oxidized zirconium split washers.

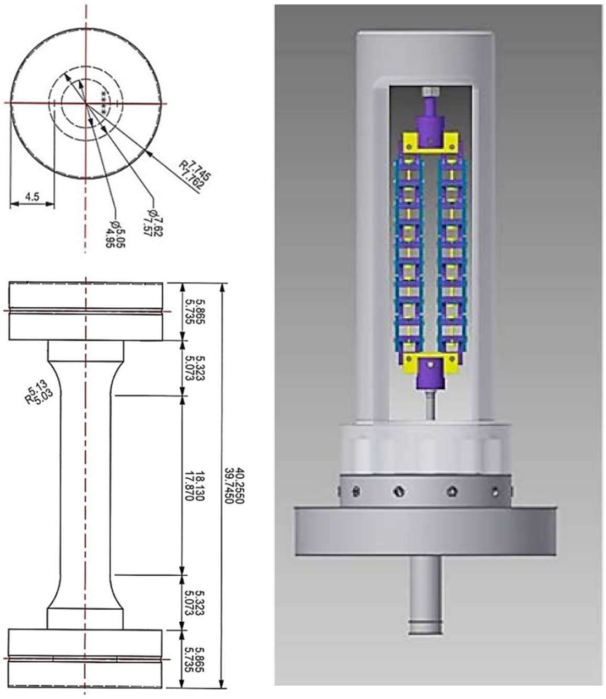

(a) (b)

Figure 2. (a) Button head specimen design. All units are in millimeters and the two values represent the accepted tolerances. (b) Loading arrangement.

The specimens were monitored for SCC initiation using direct current potential drop (DCPD), adapting a development of the method reported by Etien et al [12, 15]. The current path across multiple specimens was achieved by linking the specimens through a current bridge, in the form of a wire, between the specimens; and the potential drop across each specimen was measured. The DCPD arrangement can measure up to 5 current loops of 6 specimens each; however, for these tests, the number in each DCPD loop was limited to 2 or 3. The loops are referenced A to D, and R for the reference specimen loop. The specimens are numbered from top to bottom in the load chain. Reference specimens are included so that any change in material resistivity with time in high temperature water environments, particularly for nickel-based alloys, can be observed and, if necessary, accounted for. The reference specimens are not loaded, so changes to the DCPD are not a result of crack growth. The initiation time is identified by the inflection point on the DCPD response. For the specimens used in these tests, SCC initiation can be identified from cracks ~200μm in depth; this correlates typically to a surface crack 400-500 μm in length.

The ECP of a specimen and a Pt wire were monitored by an Ag/AgCl external pressure balanced reference electrode.

Crack Initiation Testing in of Stainless Steel in Water Chemistry Pairs (D, J; CF~100) and (M, N; CF=20) [Lucideon M+P Lab, USA]

SCC initiation tests were performed in two 4-liter Hastelloy C-276 autoclaves, one for tests in the B/Li chemistries and one for tests in the B/K chemistries. Each autoclave contained ten specimens (Figure 1b) fabricated from ~20% CW Type 304 stainless steel (heat AJ9139, the same heat was used in crack growth rate testing); Table 7 provides the mechanical properties, which were used to determine the loads to deliver the target applied stresses in the crack initiation tests. After ~20% forging reduction at 240°C of the 304SS, threaded round tensile specimens (Figure 1c) were machined to a gage diameter of 0.232 inch (5.89 mm), with a standard deviation in their diameters of 0.0003 inch (7.6 μm). The gauge diameter is perpendicular to the direction of forging thickness reduction and to the direction of applied stress during testing. The specimens were numbered to track them.

Table 7. Tensile data in air at 350°C of the 20.7% forged 304SS (heat AJ9139).

	Yield Strength, MPa	Tensile Strength, MPa	% Elongation	% Reduction in Area
Specimen 1	360.9	521.2	22.5	68.0
Specimen 2	374.2	521.9	22.0	67.4
Average	367.6	521.6	22.3	67.7

After assembly and spot welding Pt DCPD wires, the system was closed, purged with nitrogen, filled with hydrogen saturated water chemistry, and run at a water flow rate of 100 cc/min during and after heat up to the target temperature of 350°C. Like the crack growth rate testing that was also performed at Lucideon M+P Laboratory, the dissolved hydrogen concentration in the crack initiation tests was 19 cc/kg H_2 (1.7 ppm). In each system, the 10 specimens were distributed in two loading strings (five specimens per string). The applied stresses are calculated based on specimen diameter, load applied by the system pressure, and load applied by the servo-electric system. A ball joint outside the autoclave distributed the applied load equally to each loading string. The pull rods and pressure seals were 3/8" (9.53 mm) diameter, and at a system pressure of 2800 psi (19.3 MPa) the internal pressure applied 309 pounds (1.37 kN) on each pull rod, and this load was accounted for in the load applied by the servo-electric system. For the initial loading of the specimens, the load was increased over a few minutes to 90% of the yield strength (YS), then a 24-hour ramp was used to achieve the initial target load. In the latter part of most tests, the stress was increased progressively.

Crack initiation was monitored by DCPD, using the same instruments and general techniques as for crack growth. The platinum potential wires were spot welded to the radius just outside the gage length of each specimen. The system design distributed the reversed DC current through the autoclave and internal load stand structures, with the circuit completed through the specimens and down the pull rod, which was insulated from the loading system. Current reversal occurred about every 0.25 second and is designed to eliminate measurement errors associated with thermocouple effects. Crack initiation is determined from the inflection point in the DCPD potential vs. time. In all cases where DCPD detected crack initiation, it was confirmed by actuator position, consistent with prior tests [11,16-20], although the DCPD data provided somewhat better resolution.

When initiation occurred, the servo loading was removed before cooling, although often the load dropped significantly or to zero as a result of SCC initiation and growth, or specimen failure. The autoclave was cooled and opened, and the initiated/failed specimen was replaced by a dummy specimen. The same procedure as for initial loading was used to close, purge, fill and heat the autoclave, but after loading to 90% YS, a 1-hour ramp was used to achieve the target load. After the load was increased to 90% YS,

the maximum servo-electric actuator rate was limited to 0.001 inch/minute to avoid any sudden changes in loading from noise.

DCPD voltage resolution in a given system does not directly translate to the minimum crack size that can be detected because it also depends strongly on the cross-sectional area of the specimen and the gage length (distance between DCPD potential probes). If the distance between probes is roughly two or three times the specimen diameter, a crack representing about 0.1-0.2% of the specimen area can be detected under optimal situations; however, under the practical situations of this study, the detection limit correspond approximately to a semicircular crack in the range of 0.005-0.010 inch (127-254 μm) surface length, whose depth is approximately half the surface length.

Like the crack growth rate tests, the corrosion potentials of the specimens were monitored by a ZrO_2 membrane electrode (which depends on pH_T) and a Pt electrode (which depends on pH_T and H_2).

RESULTS

Crack Growth Rate Testing of Stainless Steel across a Range of Concentration Factors [Lucideon M+P Lab, USA]

Crack growth rate testing was conducted for pairs of equimolar water chemistries that span the range of concentration factors and pH_T in Table 1 to efficiently assess whether and/or when differences between LiOH vs. KOH may be observed, by changing the water chemistry on-the-fly; for example, stable crack growth response was obtained at constant stress intensity in a LiOH-based water chemistry, then the corresponding KOH-based water chemistry was introduced into the autoclave to displace the previous water chemistry, without disrupting the test.

SCC growth rate testing was performed using two 1T CT specimens in tandem: one of ~20% CW Type 304 SS (heat AJ9139) and one of ~20% CW Type 321 SS (heat E6376). In the tandem arrangement, if crack growth rate responses of the two specimens with respect to stress intensity are comparable, then the response of the two specimens will remain comparable throughout the test, thus providing two "duplicate" datasets in parallel. Unfortunately, the crack growth rate of the two specimens were significantly different, which led to the sequential collection of data; first by controlling the stress intensity factor of the Type 321 SS specimen, which had the faster crack growth rate, until its available ligament had been consumed and it was removed from the autoclave; and then by controlling the stress intensity factor of the Type 304 SS specimen. Because the Type 304 SS had the lower crack growth rate, traversing its available ligament took a longer time, which offered more opportunities for on-the-fly water chemistry changes; therefore, there are more datapoints in Figure 3 (the 304 SS specimen) than Figure 4 (the 321 SS specimen). Figure 3 and Figure 4 plot for each water chemistry pair the ratio:

$$\frac{\text{Crack growth rate in the KOH-based water chemistry of the pair}}{\text{Crack growth rate in the LiOH-based water chemistry of the pair}}$$

In a well-controlled test, crack growth rates that differ by a factor of 2 or less are considered comparable.

Figure 3 (the 304 SS specimen) shows that:

- In the water chemistry pairs (E, K; CF=316) and (D, J; CF~100), the ratio is high; that is, the crack growth rates in the KOH-based water chemistry in each pair is significantly higher than in the LiOH-based water chemistry.
- For the water chemistry pair (C, I; CF~30) and (B, H; CF~10), the crack growth rates are comparable in the KOH-based and LiOH based water chemistries of each pair.

Figure 4 (the 321 SS specimen) has only data for the water chemistry pair (E, K; CF=316), but it corroborates the data in Figure 3, that the ratio is high; that is, the crack growth rates in the KOH-based

water chemistry is significantly higher than in the LiOH-based water chemistry. This result substantiates that the performance difference observed in Type 304 SS also occurs in Ti-stabilized austenitic stainless steel, a grade consistent with the Russian steel used in VVERs.

Table 8 and Table 9 compile the crack growth rates and provide the ratios plotted in Figure 3 and Figure 4. Figure 5 and Figure 6 provide the associated DCPD traces.

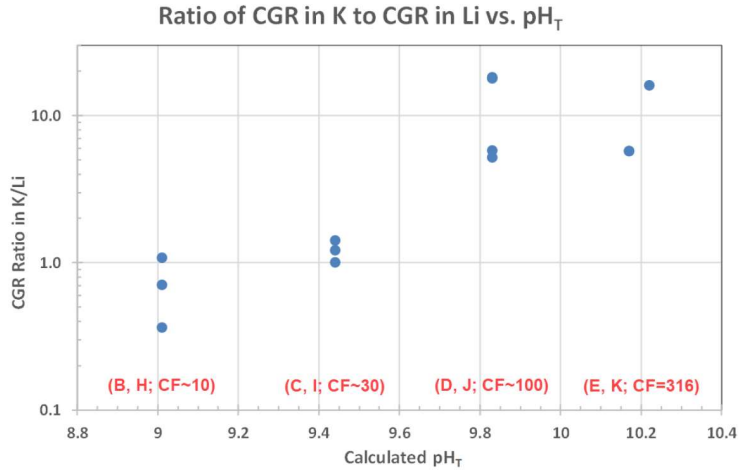

Figure 3. The (ratio of the SCC growth rate in the B/K chemistry to the B/Li chemistry) vs. pH$_T$ of the ~20% CW Type 304 stainless steel specimen (C819), using the most compelling, reproducible data collected from the specimen. [Note: There are two data points in Table 8 that are not visible in this figure because of overlap.] The reader should focus on the labels for the water chemistry pairs and their concentration factors (CF), because a different software was used to calculate pH$_T$ values, which can differ somewhat from the MULTEQ values in Tables 1, 8, and 9.[6]

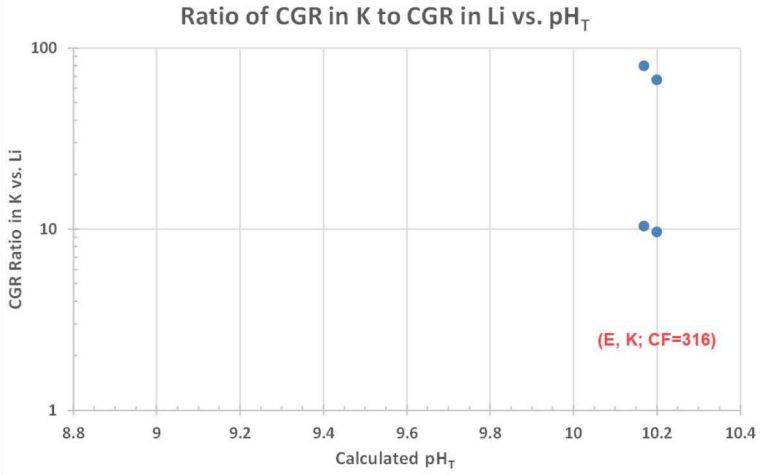

Figure 4. The (ratio of the SCC growth rate in the B/K chemistry to the B/Li chemistry) vs. pH$_T$ of 20% CW Type 321 stainless steel (C820) using the most compelling, reproducible data collected from the specimen. The reader should focus on the labels for the water chemistry pairs and their concentration factors (CF), because a different software was used to calculate pH$_T$ values, which can differ somewhat from the MULTEQ values in Tables 1, 8, and 9.[6]

[6] The largest differences are 0.18 pH for Chemistry C (with MULTEQ having the lower pH$_{350C}$ value) or 0.16 pH for Chemistry K (with MULTEQ having the higher pH$_{350C}$ value).

Table 8. Summary of Key SCC Growth Rates Transitions for ~20% CW 304 SS, Specimen C819. All data include 143 ppm B as H_3BO_3.

Chemistry Transition	Before Transition				Time of Transition Hour	After Transition				CGR Ratio KOH/LiOH
	pH 350C	Li ppm	K ppm	CGR mm/s		pH 350C	Li ppm	K ppm	CGR mm/s	
B (O_2 → H_2)	9.01	7.26	0	1.60E-06	322	Same but 2ppm O_2 →19cc/kg H_2 (1.7ppm)			3.00E-07	N/A
K → E	10.17	0	1349	1.60E-06	3927	10.2	238	0	2.80E-07	5.71
E → K	10.2	238	0	2.80E-07	4361	10.17	0	1349	1.60E-06	5.71
K → E	10.17	0	1349	1.60E-06	4772	10.2	238	0	1.00E-07	16
E → D	10.2	238	0	1.00E-07	5249	9.83	74.4	0	4.40E-08	N/A (both LiOH chemistries)
D → J	9.83	74.4	0	4.40E-08	5513	9.83	0	421	8.00E-07	18.18
J → D	9.83	0	421	8.00E-07	5920	9.83	74.4	0	4.50E-08	17.78
D → J	9.83	74.4	0	4.50E-08	6210	9.83	0	421	2.60E-07	5.78
J → D	9.83	0	421	2.60E-07	6781	9.83	74.4	0	5.00E-08	5.20
D → C	9.83	74.4	0	5.00E-08	7287	9.44	23.2	0	1.20E-8	N/A (both LiOH chemistries)
C → I	9.44	23.2	0	1.20E-08	7622	9.44	0	131.7	1.70E-8	1.42
I → C	9.44	0	131.7	1.70E-8	7961	9.44	23.2	0	1.40E-08	1.21
C → I	9.44	23.2	0	1.40E-08	8414	9.44	0	131.7	1.40E-8	1.00
I → B	9.44	0	131.7	1.40E-8	8801	9.01	7.26	0	1.10E-8	N/A (not equimolar pair)
B → H	9.01	7.26	0	1.10E-8	9207	9.01	0	41.2	4.00E-9	0.36
H → B	9.01	0	41.2	4.00E-9	9587	9.01	7.26	0	3.70E-9	1.08
B → H	9.01	7.26	0	3.70E-9	10049	9.01	0	41.2	2.60E-09	0.70

Note: pH calculated using pHsc4 software version 4.02 (Feb 19, 1997)

Note: There is a transition between the equimolar pair D → J at 1045h that is not included in this table because it was a single transition, not verified by successive repeats, and the response of the specimen was not consistent early in the test.

Table 9. Summary of Key SCC Growth Rate Transitions for ~20% CW 321 SS, Specimen C820. All data include 143 ppm B as H_3BO_3.

Chemistry Transition	Before Transition				Time of Transition Hour	After Transition				CGR Ratio KOH/LiOH
	pH 350C	Li ppm	K ppm	CGR mm/s		pH 350C	Li ppm	K ppm	CGR mm/s	
B (O_2 → H_2)	9.01	7.26	0	1.80E-06	322	Same but 2ppm O_2 →19cc/kg H_2 (1.7ppm)			3.00E-07	N/A
K → E	10.17	0	1349	9.30E-06	2258	10.2	238	0	9.60E-07	9.69
E → K	10.2	238	0	9.60E-07	2568	10.17	0	1349	1.00E-05	10.42
K → E	10.17	0	1349	1.00E-05	2689	10.2	238	0	1.50E-07	66.67
E → K	10.2	238	0	1.50E-07	2928	10.17	0	1349	1.20E-05	80.00

Note: pH calculated using pHsc4 software version 4.02 (Feb 19, 1997)

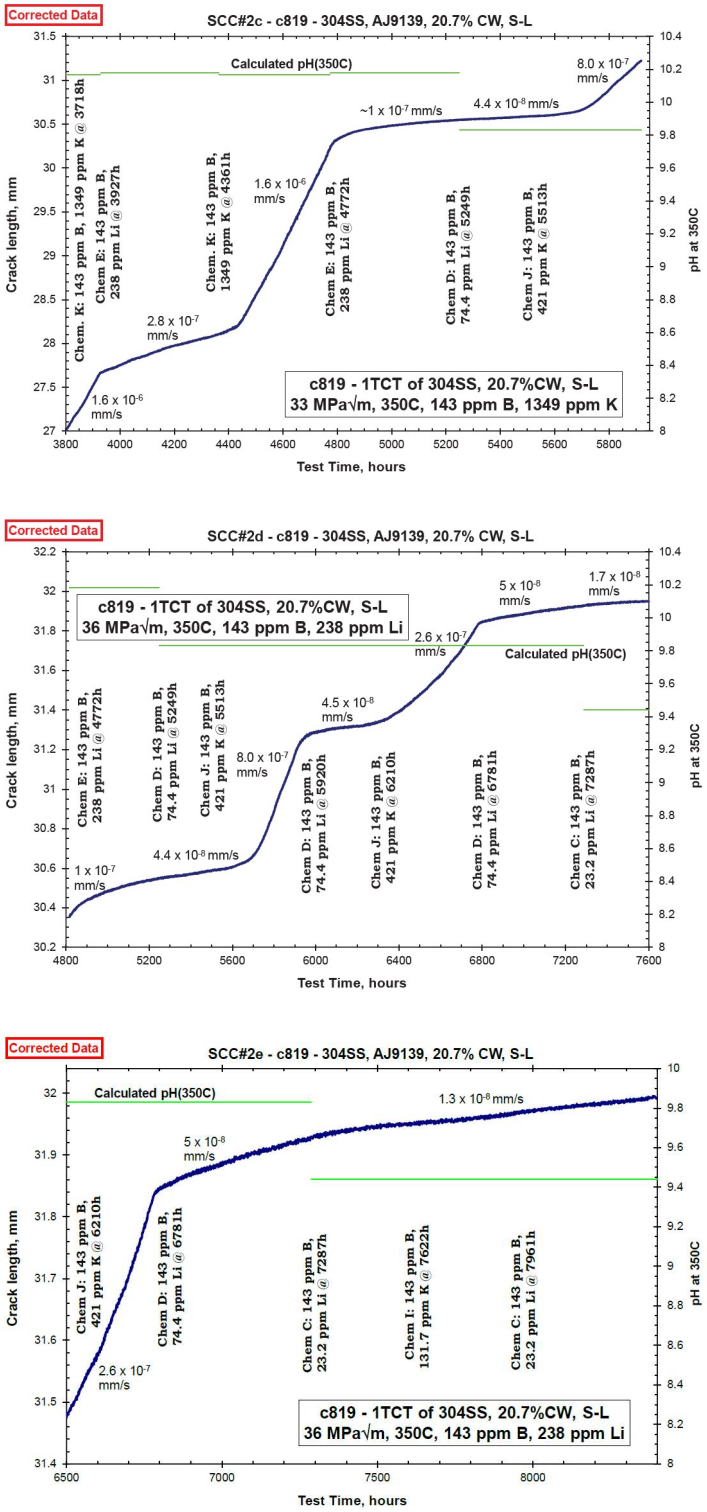

Figure 5 (Continued next page). SCC response of 304 SS specimen C819 during various chemistry changes. Note: The legend in each plot refers to the corrected stress intensity factor at the beginning of the plot.

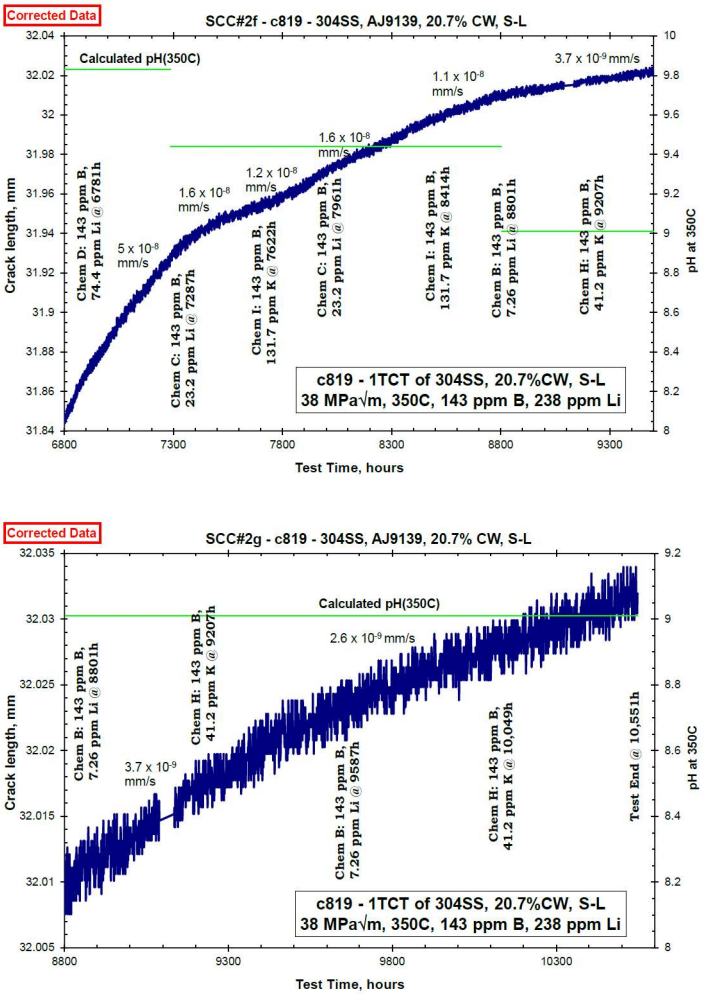

Figure 5 (Continued). SCC response of 304 SS specimen C819 during various chemistry changes. Note: The legend in each plot refers to the corrected stress intensity factor at the beginning of the plot.

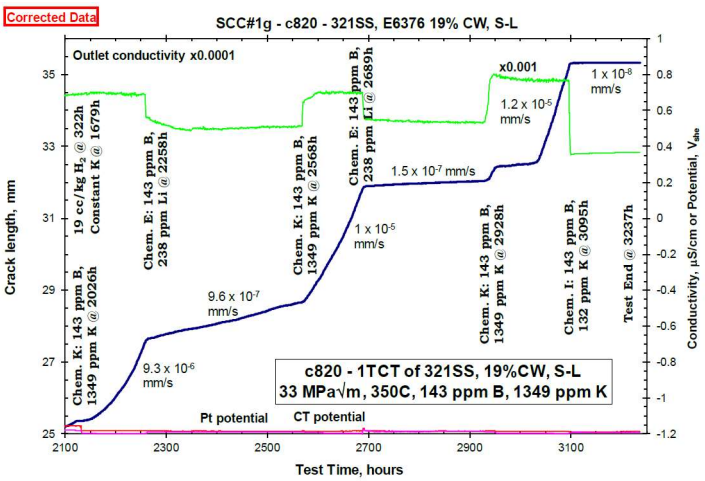

Figure 6. SCC response of 321 SS specimen C820 during various chemistry changes. (Dark blue: crack length; green: conductivity; red: CT potential; lavender: Pt potential). The label “Constant K” refers to “constant stress intensity factor”, not Potassium. Note: The 33 MPa√m in the legend refers to the corrected stress intensity factor at the beginning the plot.

Crack Initiation Testing of Alloy 600 in Water Chemistry Pair (E, K; CF=316) [Amentum, UK]

Identical tests were conducted in two autoclaves, one for the LiOH-based water chemistry and one for the KOH-based water chemistry, each containing ten specimens, for the same duration of 3275 hours "at temperature at load". The tests started at 340°C; during the tests, the applied strain and the temperature were increased to encourage initiation as identified by the sequence in Table 10.

Table 10. Crack initiation test sequence for Alloy 600 in Water Chemistry Pair (E, K; CF=316)

Time at temperature at load (hours)	Test Parameters
0	340°C Applied strain 0.3-0.5%
~2120	Increase target strain to 1.5%
~2560	Increase temperature to 350°C
~2920	Increase target strain to 5%
3275	End of test

The DCPD response from the two tests cannot confidently be interpreted as a statistically significant difference in crack initiation time since, in the two tests, there was only one DCPD-detected initiation, at 3020 hours "at temperature at load" in the KOH autoclave (Specimen APU17 at location C2), that was assigned a high confidence level.

Because there were insufficient DCPD-detected initiations for a statistically significant quantitative comparison of Alloy 600 in the water chemistry pair (E, K; CF=316), post-test inspection was conducted. Post-test inspection did find cracks, but they were below the sensitivity of DCPD detection.

- On specimens tested in KOH crevice chemistry, the surface crack density is substantially higher (Figure 7).
- However, based on examination of serially polished longitudinal cross-sections from a subset of specimens, the depths distributions of the cracks from the KOH and LiOH crevice chemistry tests were not very different (Figure 8 and Figure 9).
  - Although the cracks in the KOH crevice chemistry test were more numerous, upon sectioning, they appeared to be mostly <100 μm in depth.
    - The deepest crack in KOH was ~388 μm, although, in some cases, the surface traces of the cracks are over a millimeter in length.
  - The deepest crack in the LiOH crevice chemistry test was ~228 μm.

For the specimen diameter/geometry and DCPD parameters used, it is commonly assumed that cracks can be detected once they reach ~200 μm in depth; however, this is predicated on the condition that the crack continues to propagate. For cracks that arrest, or are developing very slowly, it may not be possible to discern an inflection point on the DCPD trace with sufficient confidence to define an initiation time. This is why only one DCPD-detected initiation in the KOH autoclave was assigned a high confidence level, although Figure 9 indicates several specimens had crack depths in the range of 350-400 μm.

A key piece of additional supporting information is the crack initiation data collected within the ICG-EAC round robin on this same heat of Alloy 600. If one were to take a conservative approach and assume that the DCPD initiation times that were assigned a low confidence level in both the KOH and LiOH crevice chemistry tests were actually detected by DCPD with high confidence, then they were comparable to the initiation times obtained in standard LiOH primary water chemistry within that study (Figure 10); therefore, the KOH crevice chemistry does not appear deleterious.

To reiterate, on the basis of crack initiation time, it is not possible to say that there is an appreciable difference in EAC susceptibility between LiOH and KOH highly-concentrated crevice chemistries, although the number of surface cracks is substantially higher in the KOH crevice chemistry.

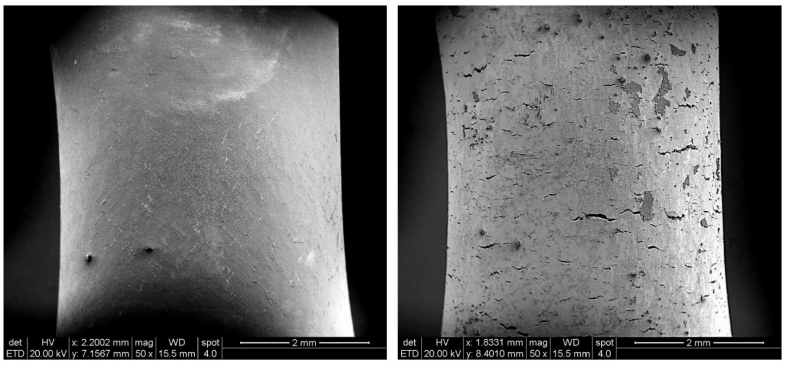

Figure 7. A comparison of Alloy 600 specimens tested in the water chemistry pair (E, K; CF=316). (Left) LiOH crevice chemistry; most surface crack lengths <200 μm. [They can be more clearly distinguished by using a higher PDF magnification.] (Right) KOH crevice chemistry.

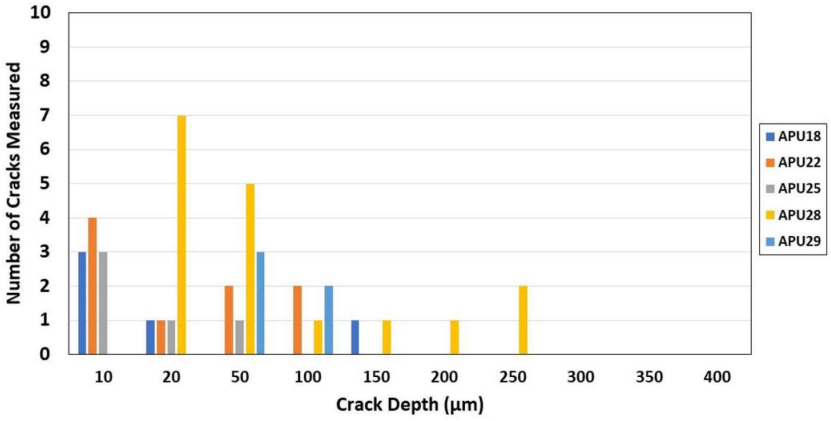

Figure 8. Distribution of crack depths found in selected Alloy 600 specimens that had been tested in LiOH water chemistry E (CF=316) and subsequently sectioned.

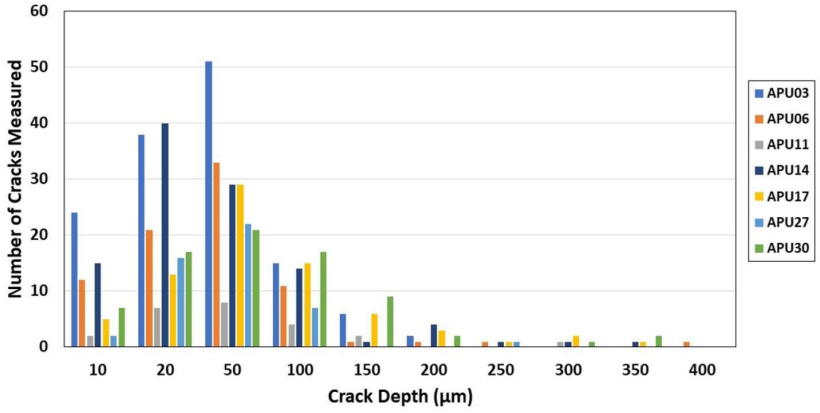

Figure 9. Distribution of crack depths found in selected Alloy 600 specimens that had been tested in KOH water chemistry K (CF=316) and subsequently sectioned; because the surface crack density is higher and seven specimens are plotted (compared with five), the distribution is more “filled-in” than that of the specimens tested in LiOH water chemistry E (CF=316).

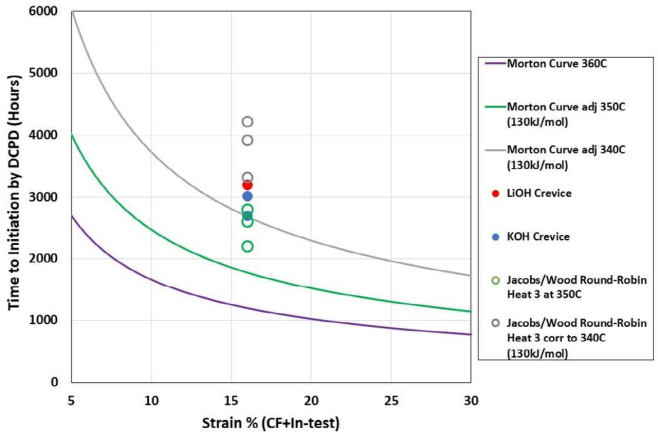

Figure 10. Comparison of the measured possible initiation times in the water chemistry pair (E, K; CF=316) [assuming the cracks were to propagate] with the initiation times for this heat of Alloy 600 in LiOH standard conditions at 350°C (and also adjusted to 340°C using 130 kJ/mol activation energy) measured by the ICG-EAC Round Robin [21]. Also shown is the Morton curve from Reference [12], adjusted for temperature.

Crack Initiation Testing of Stainless Steel in Water Chemistry Pair (E, K; CF=316) [Amentum, UK]

Identical tests were conducted in two autoclaves, one for the LiOH-based water chemistry and one for the KOH-based water chemistry, each containing ten specimens. The test temperatures were 350°C, and specimens were loaded to achieve a strain of 0.8-1.4%; these conditions were maintained for the duration of the tests. The temperature and strain values were informed by the Alloy 600 tests, and the desire to prevent impractically long test durations.

The behaviors of the specimens in the LiOH and KOH crevice chemistries were clearly different.

- In the KOH crevice chemistry, DCPD detected initiation in eight of ten specimens after 430 hours; the test ended shortly thereafter (Figure 11).
- In the LiOH crevice chemistry, there were no DCPD-detected initiations when the test ended after 1410 hours (Figure 12).

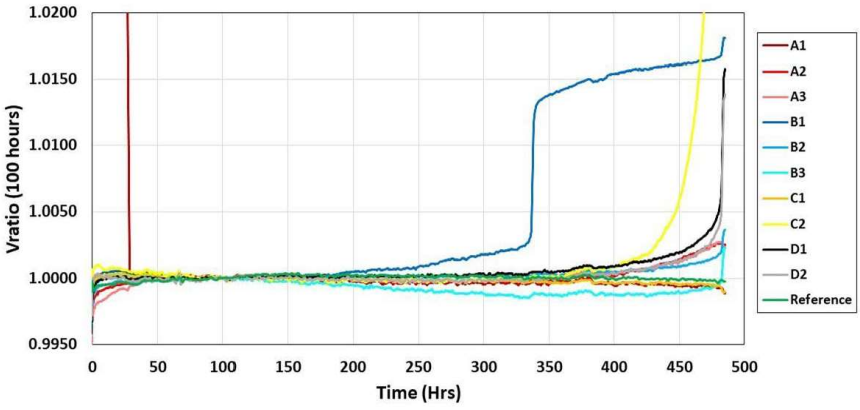

Figure 11. DCPD summary using voltage ratio (at 100 hours) for all 304L specimens tested in the KOH crevice chemistry K (CF=316). Note that eight out of the ten specimens exhibit the upward inflection of its DCPD trace that is indicative of crack initiation; the two that did not were A1 and C1. (The ten specimens do not include the non-stressed “reference” specimen.)

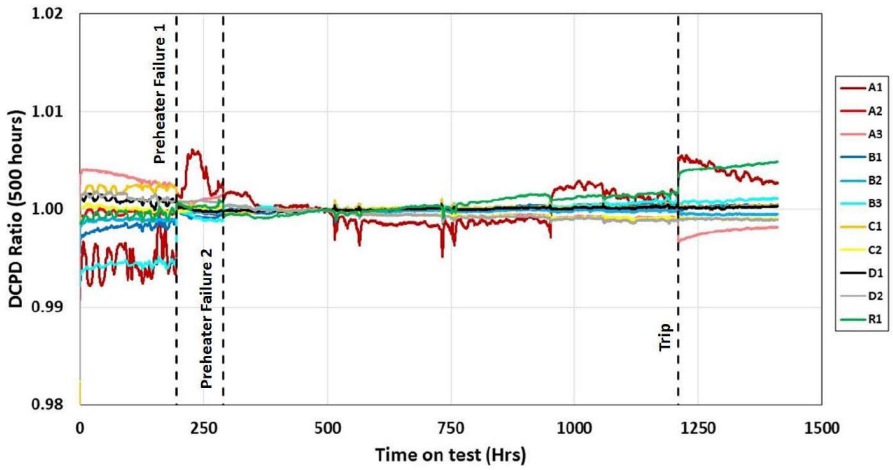

Figure 12. DCPD summary using voltage ratio (at 500 hours) for all 304L specimens tested in the LiOH crevice chemistry E (CF=316). No specimen exhibits an upward inflection to its DCPD trace that is indicative of crack initiation.

Post-test inspection also found clear differences.

- In the KOH crevice chemistry:
  - Substantial surface cracking was observed in eight out of the ten specimens for which DCPD detected initiation.
    - Only small, isolated cracks (<200 μm surface length) were observed on the other two specimens.
  - The depth distribution of the cracks from observation of serially polished longitudinal cross-sections is provided in Figure 13.
- In the LiOH crevice chemistry:
  - Only three features that may be intergranular cracks were identified on two out of the ten specimens, and they were <100 μm in surface length.
  - A meaningful depth distribution could not be obtained because of the small number of features.
  - The cracks were clearly below the depth resolution of DCPD.[7]

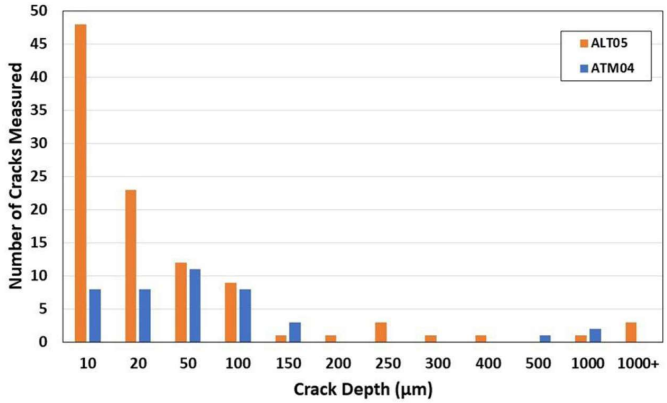

Figure 13. Distribution of crack depths found on the sectioned 304L specimens ALT05 (C2) and ATM04 (D1) tested in the water chemistry pair (E, K; CF=316).

[7] At the time of DCPD detection of initiation, the aspect ratios (depth/surface length) were approximately 0.5 or less.

Figure 14 shows the ECP measured between a platinum wire placed in the autoclave and an Ag/AgCl external pressure balanced reference electrode, for 4 crevice tests [Alloy 600 in KOH and in LiOH; 304L in KOH and in LiOH]; some small deviations in the measured potentials, associated with test start/interruptions, have been removed. The average potentials, shown by the dashed lines, support a difference in potentials between the two chemistries of 25 to 40 mV, depending on the value compared. For a pH dependence at 350°C of (123.6 mV/pH unit) a pH_T difference of 0.2 to 0.32 could be inferred, where the KOH crevice chemistry has the higher pH_T. This measurement is supportive but not definitive, as it was not designed to determine ΔpH_T.

- In Table 1, MULTEQ calculates a pH_T difference of 0.13 [water chemistry pair (E, K)], where the KOH crevice chemistry has the higher pH_T.

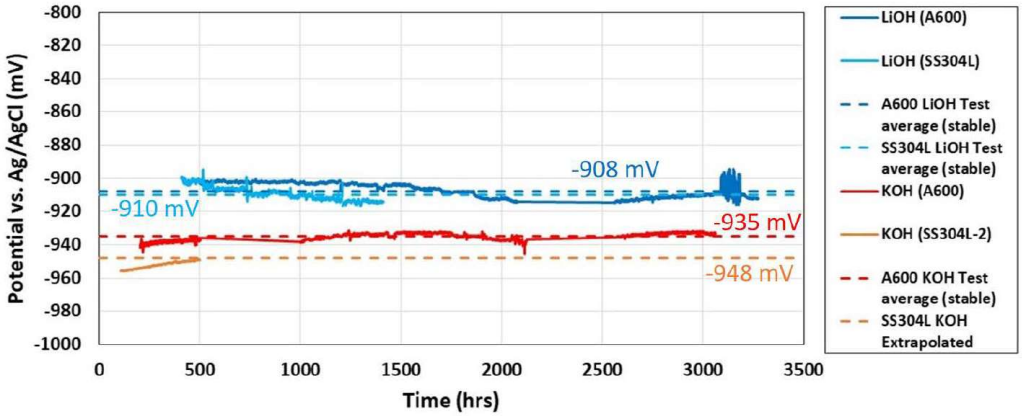

Figure 14. Electrochemical potential measured between Pt and an Ag/AgCl reference electrode for the crevice tests in the water chemistry pair (E, K; CF=316), with deviations from test start/restart removed. The dashed lines show the average potential for the respective tests, with the exception of KOH (SS304L-2), which extrapolates a potential from the end of the test at 500 hours. Values are shown in the respective colors. A ΔpH_T of 0.2 to 0.32 could be inferred, where the KOH crevice chemistry has the higher pH_T.

<u>Crack initiation testing of Type 304 Stainless Steel in Water Chemistry Pair (D, J; CF~100) [Lucideon M+P Lab, USA]</u>

As Table 11 and Table 12 indicate, for this pair of tests, the durations at-temperature-and-load of different stages of loading conditions were approximately 850 hours at 105% YS (yield strength), approximately 340 hours at 120% YS, and different times at 125% YS. The total at-temperature-and-load test durations (all testing at a temperature of 350°C) were 3127 hours in the LiOH-based water chemistry (Chemistry D) and 1742 hours in the KOH-based water chemistry (Chemistry J).[8]

The total at-temperature-and-load test durations (3127 hours in LiOH vs. 1742 hours in KOH) were different because:

- In the LiOH-based water chemistry, the test continued for a duration of 1936 hours (at-temperature-at-load) at 125% YS, the last and highest stress level, after which the test was ended with no DCPD-detected initiations.

[8] A 3-specimen exploratory crack initiation test was conducted in Water Chemistry J (KOH-based) to inform the stress levels for testing. Because Water Chemistry Pair (D, J; CF~100) is less aggressive than (E, K; CF=316), a higher level of mechanical acceleration was anticipated to be necessary to mitigate the possibility of no initiations in both members of the pair.

- In the KOH-based water chemistry, the test was ended after DCPD detected initiation in half of the specimens, which occurred after a duration of 552 hours (at-temperature-at-load) at 125% YS.

The DCPD data shows that crack initiation behavior in KOH-based Chemistry J is worse than in LiOH-based Chemistry D (both at a concentration factor of ~100).

- This is consistent with the higher crack growth rates in KOH-based Chemistry J than in Chemistry D (Figure 3 and Table 8).

Although the DCPD data is unambiguous, post-test examination was conducted and identified cracking (below the depth resolution of DCPD) in some specimens without DCPD-detected initiation:

- In the LiOH-based water chemistry (Chemistry D), post-test inspection identified cracks in 6 out of the 10 specimens. (There were no DCPD-detected initiations.) [Table 13]
- In the KOH-based water chemistry (Chemistry J), post-test inspection identified cracks in 4 specimens.
  - In total, DCPD detected cracking in 5 specimens and post-test inspection detected cracking in a further 4 specimens, out of 10 specimens. [Table 14]

Table 11. Loading during crack initiation test in Chemistry D (143 ppm B and 74.4 ppm Li, and 19 cc/kg hydrogen). [Chemistries D and J are equimolar pairs with CF~100.] “Data Acq. Time” includes time not "at temperature at load” (e.g., if there were some test interruptions).

Start Data Acq. Time, h	At T at Load Start Time[(i)], h	At T at Load Duration[(i)], h	Loading Condition as a % of Yield Strength
127	0	859	Constant load at 105% YS
1168	859	332	Constant load at 120% YS
1499	1191	1936	Constant load at 125% YS
3435			End of Test
		Total: 3127	

(i) Because there were test interruptions during first loading condition, the “At T at Load Start Time” values and some “At T at Load Duration” values cannot be deduced from “Start Data Acq. Time” simply by subtraction.

Table 12. Loading during crack initiation test in Chemistry J (143 ppm B, 421 ppm K, and 19 cc/kg hydrogen). [Chemistries D and J are equimolar pairs with CF~100.] “Data Acq. Time” includes time not “at temperature at load” (e.g., if there were some test interruptions).

Start Data Acq. Time, h	At T at Load Start Time[(i)], h	At T at Load Duration[(i)], h	Loading Condition as a % of Yield Strength
127	0	846	Constant load at 105% YS
1056	846	344	Constant load at 120% YS
1400	1190	552	Constant load at 125% YS
2096[(ii)]			End of Test
		Total: 1742	

(i) Because there were test interruptions, the “At T at Load Start Time” values and some “At T at Load Duration” values cannot be deduced from “Start Data Acq. Time” simply by subtraction.

(ii) The initiation and failure process of Specimen #1 tripped a position limit sensor at 2096 hours, and the applied load dropped by ~85%. The test was not cooled until 2105 hours and the specimen was subsequently removed. The load was not at the target value after 2096 hours, so this table indicates that the test effectively ended at 2096 hours.

Table 13. Specimens and their time to Initiation in Chemistry D (143 ppm B and 74.4 ppm Li, and 19 cc/kg hydrogen). [Chemistries D and J are equimolar pairs with CF~100.] There was no DCPD indication of initiation (crack depths below the resolution of DCPD).

Test	Chem	Specimen (SCC severity)	Time (hours) at ≥105%YS *	Time (hours) At Final and Highest Load *
KOH6	B/Li	#20 - quite high density of IG SCC cracks up to 3 mm in length (post-test inspection)	2977(i)	1786.2(i)
		#15 - quite a few 0.5 - 2 mm cracks (post-test inspection)	3027(i)	1836.2(i)
		#19 - a few 50 - 1000 µm cracks (post-test inspection)	3027(i)	1836.2(i)
		#16 - unclear; maybe a few 50 - 100 µm cracks that are not straight (post-test inspection)	3097(i)	1906.2(i)
		#17 - likely some 50 - 150 µm cracks (post-test inspection)	3097(i)	1906.2(i)
		#18 - likely some 50 - 150 µm cracks (post-test inspection)	3097(i)	1906.2(i)

* The durations (time) in this table are time-at-temperature-and-load and differ from "data acquisition time".

(i) There were no DCPD-detected initiations in test KOH6. These specimens were determined to have initiated by post-test inspection (with crack depths below the resolution of DCPD). The test ran for 3127 hours; therefore, all these specimens were assigned initiation times of ~3000 hours (time at ≥105% YS), differing somewhat arbitrarily from 3127 hours, as it is necessary to have a distribution in time in to apply Weibull analysis (not reported in this paper). Specimens were assigned somewhat shorter or longer initiation times according to the severity of their cracking, assessed by post-test inspection. Because there were no interruptions of the test to remove initiated specimens, the time at final and highest load was obtained by subtraction the duration of the previous loading stages (1190.8 hours) from the (time at ≥105% YS) [105% YS was the lowest load tested].

Table 14. Specimens and their time to initiation in Chemistry J (143 ppm B, 421 ppm K, and 19 cc/kg hydrogen). [Chemistries D and J are equimolar pairs with CF~100.] The entries indicate whether cracking was detected by DCPD, or by post-test inspection because there was no DCPD indication of initiation (crack depths below the resolution of DCPD).

Test	Chem	Specimen (SCC severity)	Time (hours) at ≥105%YS *	Time (hours) At Final and Highest Load *
KOH7	B/K	**#2 - failure, severe cracking (DCPD-detected)**	**1411**	**211**
		#7 - severe cracking (DCPD-detected)	**1482**	**292**
		#8 - failure, severe cracking (DCPD-detected)	**1560**	**370**
		#3 - failure, severe cracking (DCPD-detected)	**1603**	**413**
		#1 - severe cracking (detected by actuator motion)(i)	**1682**	**492**
		#6 - significant cracking (post-test inspection)	1686(ii)	496(ii)
		#9 - extensive SCC cracking (post-test inspection)	1690(ii)	500(ii)
		#4 - small SCC cracks (post-test inspection)	1700(ii)	510(ii)
		#10 - many small IG SCC cracks (post-test inspection)	1700(ii)	510(ii)

* The durations (time) in this table are time-at-temperature-and-load and differ from "data acquisition time".

(i) SCC initiation of Specimen #1 was detected by actuator motion alone; the DCPD signal had become noisy, probably because a wire(s) had become detached.

(ii) DCPD did not detect initiations in Specimen #6, #9, #4, and #10. These specimens were determined to have initiated by post-test inspection (with crack depths below the resolution of DCPD). The test ran for 1742 hours; therefore, all these specimens were assigned initiation times of ~1700 hours (time at ≥105% YS), differing somewhat arbitrarily from 1742 hours, as it is necessary to have a distribution in time in to apply Weibull analysis (not reported in this paper). These specimens were assigned somewhat shorter or longer initiation times according to the severity of their cracking assessed by post-test inspection.

Crack Initiation Testing of Type 304 Stainless Steel in Water Chemistry Pair (M, N; CF=20) [Lucideon M+P Lab, USA]

Based on the crack growth rate results, water chemistry pair (M, N; CF=20) was selected as appropriate for a conservative yet relevant assessment of LiOH vs. KOH crack initiation, since the concentration factor calculated within a generalized pressurizer heater support plate crevice is approximately 2 once convection is taken into account. [10] Accordingly, the CF of 20 that was tested is approximately one order of magnitude greater than the expected, limiting PWR pressurizer support plate crevice chemistry environment. for both boron and the cation species (Li or K).

The durations of different stages of loading conditions as well as the total at-temperature-and-load durations this pair of tests are provided in Table 15 and Table 16; they are essentially identical.

There were no DCPD-detected initiations, although the total at-temperature-and-load duration (all testing at a temperature of 350°C) in this water chemistry pair (M, N; CF=20) [3258 hours in both] were longer than those in water chemistry pair (D, J; CF~100) [1742 hours and 3127 hours, respectively], and although loading conditions were more aggressive. [127.5% YS was judged to be the highest stress level advisable, to mitigate against purely mechanical failure (unrelated to environmental effects) if the ultimate tensile strength (~142% YS) were exceeded locally.]

Post-test SEM evaluation shows numerous small cracks on all specimens, with no clear distinction between the two chemistries.

- The similarities in crack sizes and densities suggest strongly that there is no difference in SCC response between the B/Li and B/K chemistries.

The specimens of these two tests, all identified as having cracks by post-test inspection, are conservatively assigned overall initiation times ("Time at ≥105%YS") of 3258 hours in Table 17 (equivalent to the total duration "at temperature at load" of the tests).

Table 15. Loading during crack initiation test in Chemistry M (23.4 ppm B, 14.2 ppm Li and 19 cc/kg hydrogen). [Chemistries M and N are equimolar pairs with CF=20.] "Data Acq. Time" includes time not "at temperature at load" (e.g., if there were some test interruptions).

Start Data Acq. Time[(i)], h	At T at Load Time, h	At T at Load Duration, h	Loading Condition as a % of Yield Strength
168	0	1536	Constant load at 125% YS
1704	1536	1722	Constant load at 127.5% YS
3426	3258		End of Test
		Total: 3258	

(i) These are the times at which the ramp (~24 hours) to the target loading conditions ended and is therefore when the target loading started.

Table 16. Loading during of crack initiation test in Chemistry N (23.4 ppm B, 81.7 ppm K, and 19 cc/kg hydrogen). [Chemistries M and N are equimolar pairs with CF=20.] "Data Acq. Time" includes time not "at temperature at load" (e.g., if there were some test interruptions).

Start Data Acq. Time[(i)], h	At T at Load Time, h	At T at Load Duration, h	Loading Condition as a % of Yield Strength
49	0	1536	Constant load at 125% YS
1585	1536	1722	Constant load at 127.5% YS
3307	3258		End of Test
		Total: 3258	

(i) This is the time at which the ramp (~24 hours) to the target loading conditions ended and is therefore when the target loading started.

Table 17. Specimens and their time to initiation in Chemistry M (23.4 ppm B, 14.2 ppm Li and 19 cc/kg hydrogen) and in Chemistry N (23.4 ppm B, 81.7 ppm K, and 19 cc/kg hydrogen); CF=20. There was no consequential difference in SCC in this water chemistry pair.

Test	Chem	Specimen (SCC severity)	Time (hours) at ≥105%YS *	Time (hours) At Final and Highest Load *
KOH8	B/Li	All specimens - many small cracks (post-test inspection)	3258[(i)]	1722[(i)]
KOH9	B/K	All specimens - many small cracks (post-test inspection)	3258[(i)]	1722[(i)]

* The durations (time) in this table are time-at-temperature-and-load and differ from "data acquisition time".

(i) There were no DCPD-detected initiations in these two tests. At the end of the tests, all specimens in both tests had many small cracks (with crack depths below the resolution of DCPD), without clear differences in the crack sizes or densities between the tests.

As can be observed in Table 15 and Table 16, the stress applied to specimens in the water chemistry pair (M, N; CF=20) started at 125% YS (and then proceeded to 127.5% YS). It was assessed that starting the test at 105% YS, as was used for the testing in water chemistry pair (D, J; CF~100), would not provide sufficient acceleration to permit differentiation of performance within a reasonable testing timeframe. It is only by testing at higher stresses for a much longer duration that initiations were observed by visual inspection (below the resolution of DCPD detection), but in all of the specimens in each member of the pair (M, N; CF=20) and without clear distinction between LiOH and KOH. This is in contrast to the testing in the water chemistry pair (D, J; CF~100), where faster crack initiation occurred in the KOH-based member of the pair.

Discussion

It is clear that relative crack growth rates (CGR ratios in Figure 3 and Figure 4) of stainless steels are correlated with the crack initiation test results; in particular:

- The higher relative crack growth rates in the KOH-based water chemistries in the pairs (E, K; CF=316) and (D, J; CF~100) are consistent with earlier initiation in those same water chemistries [Figure 11, Figure 12 and Table 13, Table 14].

- The comparable crack growth rates in KOH-based and LiOH-based water chemistry of the pairs (C, I; CF~30) and (B, H; CF~10), are consistent with comparable crack initiation behavior in water chemistry pair (M, N; CF~20), whose concentration factor is in between the first two pairs [Table 17].

There is a clear difference in the crack initiation results of 304L stainless steel in the concentrated water pairs (E, K; CF=316) and (D, J; CF~100).

In contrast, for Alloy 600 tested in the most concentrated water chemistry pair (E, K; CF=316), it is not possible to say, on the basis of crack initiation time detected by DCPD, that there is an appreciable difference in EAC susceptibility between LiOH and KOH crevice chemistries; although higher crack density and longer surface crack lengths were observed in the KOH-based water chemistry K, the crack depth distributions in the two water chemistries were similar. These observations are consistent with the interpretation that for Alloy 600, the pH_T of the water chemistry pair (E, K; CF=316) are close to the "pseudo-threshold" for caustic cracking[9], but have not yet transgressed the pseudo-threshold, and that the pH_T of the KOH-based water chemistry K was closer to the pseudo-threshold. It is well known that Ni-base alloys are more resistant to caustic cracking than stainless steels; indeed, this was the reason that (Ni-base) Hastelloy autoclaves were selected for the SCC testing in this study. A hypothetically-placed pseudo-threshold for Alloy 600 is depicted in Figure 15a, in which the pH_T values of the various water chemistries are from Table 1.

Since for stainless steels, crack growth rates are higher and crack initiations are sooner in the KOH-based water chemistry in the pair (E, K; CF=316), one might place the hypothetical pseudo-threshold for caustic cracking of stainless steels in between the pH_T values of E and K, as depicted in Figure 15a. However, this leads to inconsistency, because crack growth rates are also higher and crack initiations are also sooner in the KOH-based water chemistry in the pair (D, J; CF~100), yet their pH_T values lie below the hypothetical pseudo-threshold.

There are two possible implications of this inconsistency; they are not necessarily mutually exclusive.

(1) There are other factor(s), in addition to pH_T, affecting the SCC behavior in hydrogenated LiOH vs. KOH at elevated concentration factors.

- EPRI 302005408 [2] discusses "ion-specific effects" not captured in pH_T. In the context of pressure boundary materials, the evaluation did not expect a significant differentiation in performance, but it also noted that there has been "little testing on ion specific effects of potassium" (to which this investigation is a response).

(2) The actual ΔpH_T values between equimolar LiOH and KOH pairs are larger than the calculated values in Table 3 or the range of ΔpH_T of 0.2 to 0.32 inferred from Figure 14. In particular, if one postulates pH_{350C} values of E', K', D' and J' have a range of uncertainty as large as 0.4 units as defined in the caption of Figure 15b and illustrated therein (in opposite directions for the LiOH and KOH chemistries), then it would be possible to define a hypothetical pseudo-threshold for caustic cracking of stainless steels that would be consistent with the observations; however, there is no other basis for the postulate.

In addition, since the differences in crack growth and crack initiation behavior are no longer observable by CF~30, the factors discussed in (1) and (2) become less influential as the concentration factor decreases.

[9] "Caustic cracking' is terminology that simply notes the observed SCC occurs at comparatively high pH values and does not denote a change in fundamental mechanism at a distinct pH value. The use of "pseudo-threshold" reflects that at a lower pH, SCC initiation can still occur if the test duration is increased or if test conditions are more severe [e.g., the presence of sustained strain rate (applied or from creep)].

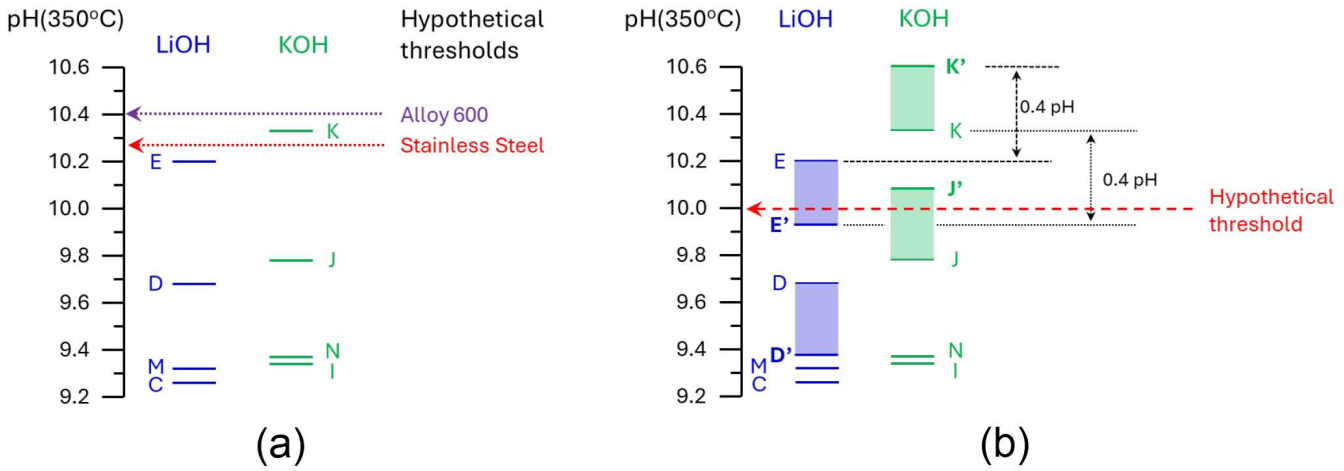

Figure 15. (a) Hypothetical pseudo-thresholds for caustic cracking of Alloy 600 and stainless steel consistent with observations in water chemistry pair (E, K; CF=316), but the hypothetical pseudo-threshold for stainless steel is not consistent with the observations in water chemistry pair (D, J; CF~100). (b) Hypothetical pseudo-threshold of caustic cracking for stainless steel, postulating an uncertainty in pH_{350C} values as large as 0.4 units; the "primed" values are determined according to: K'-E = 0.4; K-E' = 0.4; J'-D = 0.4; and J-D' = 0.4. The pH_{350C} values of the water chemistries are from Table 1. Both K' and J' (KOH-based) are located above the pseudo-threshold and would lead to crack initiation, while both E' and D' (LiOH-based) are located below the pseudo-threshold and would not lead to crack initiation. However, other than being consistent with observations, there is no other basis for the postulate.

CONCLUSIONS

The specific objective of this study is to assess whether the use of KOH vs. LiOH significantly elevates the risk of environmentally assisted cracking of the pressurizer heaters, associated with the hydrogenated concentrated crevice chemistry that may develop; the specific materials evaluated were Alloy 600 (representing Ni-base alloys) and Type 304/304L stainless steel (representing austenitic stainless steels).

With respect to this objective, the conclusions are:

- For Alloy 600, even at concentration factor of 316 [water chemistry (E, K)], it is not possible to say on the basis of crack initiation time (detected by DCPD) that there is an appreciable difference in EAC susceptibility between the equimolar LiOH and KOH crevice chemistries.
- For stainless steel, comparing equimolar solutions of LiOH and KOH at concentration factors of ~30 or lower, there is no significant impact on crack growth rates.
  - For concentration factors of ~100 and higher, higher crack growth rates are observed in the KOH-based water chemistry of an equimolar pair.
- There is a correlation between crack growth behavior and crack initiation behavior.
  - At concentration factors of ~100 and higher, higher crack growth rates are observed in KOH-based water chemistries of an equimolar pair and faster crack initiation occurs in KOH-based water chemistries of an equimolar pair.
  - At concentration factors of ~30 or less, there is no observable difference in crack growth rates between LiOH-based and KOH-based equimolar water chemistries and there are no DCPD-detected crack initiations in water chemistry pair (M, N; CF=20) nor clear differences in the crack sizes and densities on specimens' surfaces (crack depths below the resolution of DCPD).
- The combination of crack growth and crack initiation data, given the correlation between them, represents a compelling argument that no difference in crack initiation behavior should be expected

at a concentration factor of 20, although direct comparison of initiation times is not possible since there are no DCPD-detected crack initiations in the water chemistry pair (M, N; CF=20).

- A concentration factor of 20 is conservative with respect to a concentration factor of approximately 2 expected within pressurizer crevices, when convection is taken into account.

ACKNOWLEDGEMENTS

The authors acknowledge the water chemistry calculations performed by Dominion Engineering, Inc (DEI). They express sincere appreciation for the advice, feedback, and/or assistance of the following people: Peter Scott (Peter Scott Consulting), Steve Fyfitch (formerly Framatome), Martin Krondak (formerly UJV Rez), Chuck Marks (DEI), and Josh McKinley (Westinghouse).

REFERENCES

1. Potassium Hydroxide, A Potential Mitigation for AOA, EPRI, Palo Alto, CA: 1999. TE-114158.
2. Feasibility of Using Potassium Hydroxide for Primary Coolant pH_T Control in Pressurized Water Reactors. EPRI, Palo Alto, CA: 2015. 302005408.
3. K. Fruzzetti, Anne Demma, Peter Chou, Jean Smith, Dennis Hussey, Karen Kim, Carola Gregorich, Michael Burke, “Potassium Hydroxide for PWR Primary Coolant pH Control: Qualification Program”, 21st International Conference on Water Chemistry in Nuclear Power Systems, San Francisco, CA (2018): https://www.epri.com/research/products/000000003002016101
4. P. Chou, J. Smith, A, Demma, M. Burke, and K. Fruzzetti, “Potassium Hydroxide for PWR Primary Coolant pH Control: Materials Qualification Testing”, 21st International Conference on Water Chemistry in Nuclear Power Systems, San Francisco, CA (2018): https://www.epri.com/research/products/000000003002016101
5. PWR Primary Chemistry KOH Qualification: Crack Initiation and Crack Growth Testing of Non-sensitized Stainless Steel and Crack Initiation Testing of a Ni-base Alloy in Hydrogenated Crevice Water Chemistries. EPRI, Palo Alto, CA: 2024. 3002028926.
6. EPRI Materials Degradation Matrix, Revision 4. EPRI, Palo Alto, CA: 2018. 3002013781.
7. Materials Reliability Program: VVER Issue Management Tables (MRP-471). EPRI, Palo Alto, CA: 2021. 3002021033.
8. Y. Thebault, P. Moulart, K. Dubourgnoux, J. Champredonde, T. Couvant, Y. Neau, J-M. Fageon, D. Lecharpentier, A. Breuil, and V. Derouet, “PWSCC of Thermocoax Pressurizer Heaters in Austenitic Stainless Steel and Remedial Actions to Preventing SCC”, 15th International Conference on Environmental Degradation, TMS, 2011.
9. Estimation of Pressurizer Superheat, Calculation No. C-5758-00-02, Revision No. 0, November 14, 2017. Prepared by Dominion Engineering, Inc. under contract to EPRI.
10. Estimation of Pressurizer Superheat, Calculation No. C-5758-00-02, Revision No. 2, March 31, 2023. Prepared by Dominion Engineering, Inc. under contract to EPRI.
11. Stress Corrosion Cracking Testing Guidelines: With Emphasis on High Temperature Water. EPRI, Palo Alto, CA: 2020. 3002018265.
12. R.A. Etien, E. Richey, D.S. Morton and J. Eager, “SCC Initiation Testing of Alloy 600 in High Temperature Water, p2407, proceedings of 15th International Conference on Environmental Degradation of Materials in Nuclear Power Systems - Water Reactors, August, 2011, in Colorado Springs, CO.
13. Materials Reliability Program: Recommended Factors of Improvement for Evaluating Primary Water Stress Corrosion Cracking (PWSCC) Growth Rates of Thick-Wall Alloy 690 Materials and Alloy 52, 152, and Variants Welds (MRP-386). EPRI, Palo Alto, CA: 2017. 3002010756.

14. Materials Reliability Program: Mitigation of PWSCC in Nickel-Base Alloys by Optimizing Hydrogen in the Primary Water (MRP-213). EPRI, Palo Alto, CA: 2007. 1015288.
15. S.R. Pemberton, M.A. Chatterton, A.S. Griffiths, S.L. Medway, D.R. Tice and K.J. Mottershead, “The Effect of Surface Condition on Primary Water Stress Corrosion Cracking Initiation of Alloy 600” p203, Proceedings of 18th International Conference on Environmental Degradation of Materials in Nuclear Power Systems - Water Reactors, August 13–17, 2017, in Portland, Oregon.
16. PWR Primary Chemistry KOH Qualification: Alloy 600 Crack Initiation. EPRI, Palo Alto, CA: 2021. 3002020893.
17. P.L. Andresen and P. Chou, “Crack Initiation of Alloy 600 in PWR Water”, Proc. 18th Int. Symp. on Environmental Degradation of Materials in Nuclear Power Systems – Water Reactors, The Metallurgical Society, August 2017.
18. P.L. Andresen and P. Chou, “SCC Initiation and Growth in PWR Primary Water Containing KOH vs. LiOH”, Proc. 19th Int. Symp. on Environmental Degradation of Materials in Nuclear Power Systems – Water Reactors, American Nuclear Soc., August 2019.
19. PWR Primary Chemistry KOH Qualification: A-286 Crack Initiation and Crack Growth. EPRI, Palo Alto, CA: 2021. 3002020894.
20. P.L. Andresen and P. Chou, “SCC Initiation and Growth Rate Response of A-286 in B/Li and B/K Solutions at 340C”, 20th Int. Symp. on Environmental Degradation of Materials in Nuclear Power Systems – Water Reactors, AMPP, August 2022.
21. P.J. Meadows, P.L. Andresen, M.B. Toloczko W.-J. Kuang, S. Ritter, M. Bjurman, L. Zhang, M. Ernestova, A. Toivonen, F. Perosanz-Lopez, J.W. Stairmand, K.J. Mottershead, “International Round-Robin on Stress Corrosion Crack Initiation of Alloy 600 Material in Pressurized Water Reactor Primary Water” CORROSION Vol. 76, No. 8, p 719–733 (2020). https://doi.org/10.5006/3532